Reliability Optimisation and Lifetime Modelling of micro-BGA Assemblies in Harsh Environment Applications

Stoyan Stoyanov*, Paul Stewart[†] and Chris Bailey*
*School of Computing and Mathematical Sciences
University of Greenwich, Park Row, London SE10 9LS, UK
Email: s.stoyanov@gre.ac.uk
Email: c.bailey@gre.ac.uk
[†]Electronics Division, Leonardo UK Ltd, 2 Crewe Road North, Edinburgh EH5 2XS, UK
Email: paul.stewart02@leonardocompany.com

Abstract — A micro-Ball Grid Array (μBGAs) is a Chip Scale Package (CSP) architecture that becomes increasingly deployed by electronics manufacturers and used in applications ranging from consumer electronics to high-reliability and high-value equipment operated in harsh environments. In the latter case, design engineers of high-reliability electronics must develop and adopt novel assembly design solutions and new assembly materials that enhance the reliability of such commercial off-the-shelf components. This paper details the results from a comprehensive reliability test program on assessing the thermal fatigue life of μBGA board-level interconnects (quaternary alloy SnPbAgCu solder composition) and from the related physics-of-failure thermo-mechanical modelling. Several package-board assembly designs developed with rigid and compliant printed circuit board (PCB) materials, and with/ without resin application are investigated and discussed. The thermo-mechanical simulation results are used to provide insights into the solder joint physics of failure. The findings confirmed that the reliability of μBGAs can be significantly impacted through assembly design alterations, and lifetime of solder joints can be increased by factor 10X and more. The modelling predictions for solder joint damage and the experimental failure data are used to develop a lifetime model for the thermal fatigue life of μBGA and similar CSP architectures.

Keywords—micro-BGA; solder joint reliability; compliant PCB; physics-of-failure; lifetime modelling; edgebond; underfill; SnPbAgCu quaternary solder alloy.

I. INTRODUCTION

Commercial off-the-shelf Chip-Scale Packages (CSP) are increasingly used in electronics systems associated with high-reliability applications such as aerospace, automotive, rail, and oil & gas wells. These applications have very different reliability requirements compared to consumer electronics and often demand operation of the equipment under harsh environment conditions. As a result, electronics manufacturers operating in the high-reliability sector must identify, develop, and deploy stress-reducing assembly designs and failure risk mitigations for such components to meet expected lifetime requirements. There has been extensive research on reliability characterisation and design optimisation of board-level package interconnects and for a range of package types, from CSP and wafer-level package designs [1,2] to BGAs and fine-pitch flip-chip assemblies [3-5]. Solder joint fatigue models and lifetime prediction methodologies are also topics that have been extensively investigated [6]. More recently, conformal coatings and their impact on the reliability of solder interconnects have been also researched, for example the work on conformally coated BGAs by Serebreni at al. [7] and the experimental and modelling characterisation of QFN assemblies deployed in high-reliability applications by Yin et al. [8].

Published studies on μBGAs have addressed several assembly challenges related to this package type such as the reflow assembly process [9] and the mechanical property characterisation of μBGA lead-free solder joints [10]. Although investigations on μBGA solder joint reliability are also reported, published research work on this topic is limited in scope, typically concerning the reliability assessment of single assembly design [11].

This paper details an investigation on identifying and characterising assembly designs for μBGA components that optimise the thermal fatigue performance and lifetime of the board-level solder joints with quaternary SnPbAgCu composition. Different reliability improvement strategies are evaluated and discussed including alternatives to a conventional, all-rigid PCB that feature compliant material layers, edgebond and underfill resin application to the package, PCBs with solder mask defined and non-solder mask defined lands, and assembly designs with dual ball redundancy configuration. Characteristic life data obtained from accelerated temperature cycling (TC) tests and solder joint damage predictions from thermo-mechanical models are presented.

II. RELIABILITY CHARACTERISATION OF MICRO-BGAS

A. *Micro-BGA Assembly: Design Variants*

A μBGA component with a typical for this package type architecture is investigated in the study. A schematic of the package construction is detailed in Fig.1.

This work was funded by Leonardo UK Ltd, through the "Reliability and Component Integrity Analysis" project, Contract No. 4500162377.

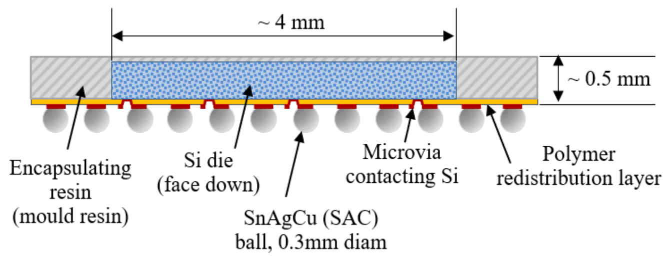

Fig. 1. Illustrative drawing of the μBGA package construction.

The μBGA size is approximately 6 x 6 x 0.5 mm. The die size land area is not matching the ball area and hence a redistribution layer is utilised to provide the required signal routing. The redistribution layer is carefully designed using a visco-elastic polymer material that provides a greater compliance between the silicon die and the solder balls. The die encapsulation using an epoxy moulding compound (EMC) is minimal, in line with the CSP package definition. The ball pitch size of the 12x12 ball grid is 0.5 mm. The grid array is nearly fully populated and features 103 solder balls.

The prime focus of the study is to investigate the reliability performance of the package type in relation to thermal fatigue failure of solder joints. The pre-assembled μBGA component is a lead-free package with SAC solder balls. When the component is attached to a PCB through a reflow process, the pre-deposited eutectic solder paste (63Sn37Pb) on the PCB pads and the package lead-free solder balls melt and mix, resulting in solder joints with quaternary alloy SnPbAgCu composition. The undertaken spectrum analysis to characterise the solder alloy composition showed that the Sn37Pb solder content in the ball alloy composition is in the range 24-28 wt.%.

Several lifetime improvement assembly designs are developed and analysed. In terms of the multi-layer PCB design, three boards are investigated:

- Rigid PCB: a conventional all-rigid stack of copper layers and "rigid" dielectric laminates, including the top-most layer beneath the solder resist at the component side of the board.
- PCB with complaint material A: The same construction as the rigid PCB but with the top layer replaced with a compliant material (A) layer stacked with the help of an adhesive layer (refer to the model illustration provided in Fig. 7, left).
- PCB with complaint material B: The same construction as the rigid PCB but with the top layer replaced with a compliant material (B) layer. No adhesive layer has been used (Fig. 7, right).

The PCB designs with compliant layers aim to provide a better compliance between the PCB and the package under temperature cycling loads by reducing deformations and stresses in the solder joints caused by the multi-material CTE mismatch. This is achieved by deployment of compliant materials that are softer compared with the "rigid" dielectric material. The three PCB variants are designed with both non-solder-mask-defined (NSMD) and solder-mask-defined (SMD) lands, with most of the assessed assembly configurations utilising the NSMD design feature. PCB layouts with dual-ball redundancy on most (but not all) joints in the grid array are considered along with a limited number of μBGA without any ball redundancy.

The second stress-reducing design strategy is exploring the potential positive effects which adhesive resins can provide. In addition to the baseline "No Resin" (NR) assembly, two additional resin-based designs are developed:

- μBGA assembly with an edgebond (EB).
- μBGA assembly with complete underfilling (UN).

The edgebond and the underfill are different materials. Fig. 2 shows cross-sections of μBGA assembly with the two resin solutions. Micro-section images from assembly specimens, that have not undergone any temperature cycling, are used to gather and confirm data related to geometric dimensions of the respective assemblies (for example the solder joints stand-off height, mould resin thickness above the die, etc.). This image data was also used to assess the cross-section profile of the edgebond and the extent to which it penetrated beneath the package edges. The extent of this penetration was found to be slightly inconsistent, typically reaching a line half-way through the second row of joints in the grid array.

mBGA Assembly with Edgebond (EB)

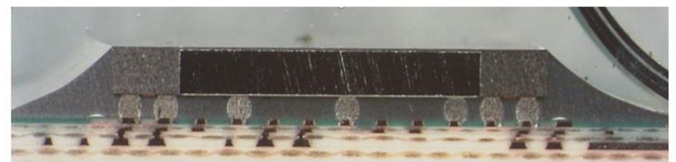

mBGA Assembly with Underfill (UN)

Fig. 2. Cross-section images of the μBGA assembly with the two resin designs: (a) edgebond (top) and (b) underfill (bottom).

Table I details the package assembly specifications reported in this paper. The nine possible combinations of the three PCB board types (rigid, compliant A, and compliant B) and the three resin options (NR, EB and UN) are all based on the dual ball redundancy and NSMD design variants of the respective boards. The resin assemblies (edgebond and underfill) have the boards with the attached μBGA components covered with conformal coating after the resin material was applied and cured.

The remaining three assemblies in Table I (Ref. 01, 02 and 05) use the rigid board design without ball redundancy. The inclusion of the three design variants in the reliability test program aimed to inform on the effects of SMD vs. NSMD PCB land type (Ref. 02 and 05) and no resin vs. edgebond impact on the reliability for PCBs with SMD pads (Ref 01 and 02).

TABLE I. REFERENCE NOTATIONS AND SPECIFICATIONS OF MICRO-BGA ASSEMBLY DESIGN VARIANTS

Ref	PCB Type	PCB Land Type	Redundant Ball/Net Design	Resin	PCB Compliant Material
01	Rigid	SMD	Single	NR	-
02	Rigid	SMD	Single	EB	-
03	Rigid	NSMD	Dual	NR	-
05	Rigid	NSMD	Single	EB	-
06	Rigid	NSMD	Dual	EB	-
08	Rigid	NSMD	Dual	UN	-
10	Compliant	NSMD	Dual	NR	A
11	Compliant	NSMD	Dual	NR	B
14	Compliant	NSMD	Dual	EB	A
15	Compliant	NSMD	Dual	EB	B
18	Compliant	NSMD	Dual	UN	A
19	Compliant	NSMD	Dual	UN	B

(N)SMD = (Non) Solder Mask Defined , NR = No resin , EB = Edgebond , UN = Underfill

B. *Reliability Testing of Micro-BGA Assemblies*

The thermal fatigue performance of the solder joints was assessed through accelerated temperature cycling (TC) tests with temperature ranging from −25°C to 100°C. The cycle time of the TC profile is 80 minutes and includes ramp up and ramp down times of 10 minutes, and dwell times of 30 minutes at the low and high temperature extreme of the cycle. The longer dwell times aimed at promoting the creep deformation of the solder joints at the respective temperature extremes.

The failure of a µBGA component due to cracking of a solder joint in the array was detected by designing a daisy chain loop connecting all critical solder joints for each individual package attached onto the board, and by continuous monitoring of the resistance change. The package fails when the measured resistance is higher than a predefined failure threshold value. The data from the daisy chain was continuously recorded and the time (cycle number) of the µBGA failure caused by failure of a critical solder joint was automatically recorded.

After the thermal cycling tests were completed, samples were cross sectioned to examine the failure mode using scanning electron microscopy (SEM) and optical microscopy. The failure mode was confirmed as solder joint fatigue cracks in the bulk solder and predominantly found near the solder/IMC interface at the component side. In some instances, cracks were also found at the PCB pad interface. Illustrative cross-sections of cracked µBGA joints under the TC test are illustrated in Fig. 3.

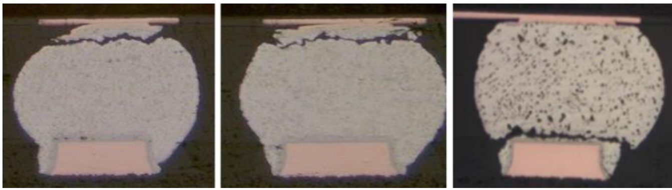

Fig. 3. Cross-section microscope images showing solder joint cracks due to thermal fatigue and caused by the accelerated TC load.

The failure data for each assembly variant detailed in Table I are gathered from component batch sizes in the range 28-32 samples per assembly case.

C. *Reliability Test Results*

The failure data is modelled using 2-parameter Weibull distributions to enable the statistical and comparative analysis of the µBGA's reliability with the different assembly designs. The Weibull distributions provided the expected characteristic life ($N_{63.2\%}$) for each assembly which was then used to compare reliability performances as well as to correlate to solder damage predictions obtained from thermo-mechanical simulations (discussed in Section III). The reported Weibull distributions and the associated 95% double sided confidence intervals are obtained in each instance using the Maximum Likelihood Estimation (MLE) method. The use of the MLE for Weibull parameters estimation is considered advantageous and recommended over the Least Squares Estimation (LSE, or rank regression) method [12]. This is particularly the case for datasets with suspensions. In such instance, the maximum likelihood technique, unlike the rank regression, considers the values of the suspensions when estimating the parameters of the distribution.

Fig. 4 shows a combined Weibull plot of the failure data obtained from the TC reliability tests. The associated characteristic life values, along with the 95% confidence interval (CI) are summarised in Table II. Most of the datasets are complete (all tested components failed). However, for several assembly designs that proved to be very reliable the TC testing was terminated before failure of all tested components in the batch is achieved, namely:

- Ref 14: 14 failures in a batch of 28 test specimen (14 suspensions).
- Ref 15: 8 failures in a batch of 28 test specimen (18 suspensions and 2 infant mortality failures).

The large number of suspensions with the above two assembly variants, particularly for Ref 15, explain the notably larger confidence intervals for the respective Weibull characteristic life parameters (see Table II).

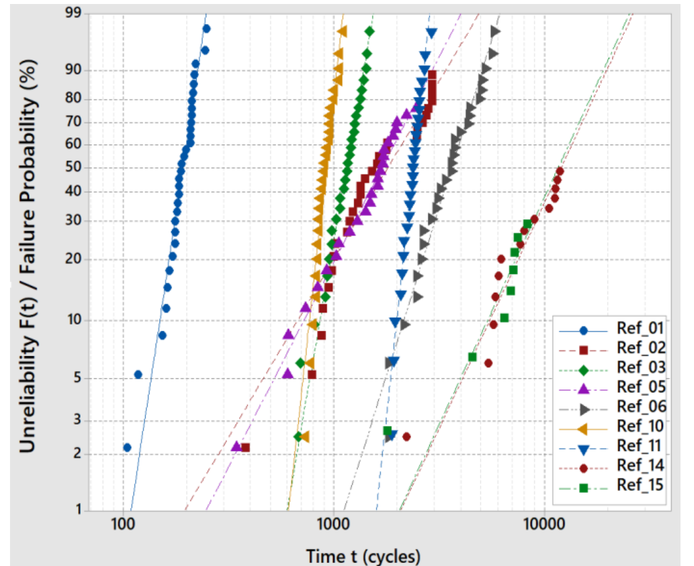

Fig. 4. Weibull distribution plots of the µBGA failure data for the 12 different package-board assembly designs in Table I.

TABLE II. TEST RESULTS FOR CHARACTERISTIC LIFE ($N_{63.2\%}$) OF THE MICRO-BGA ASSEMBLY DESIGN VARIANTS

Micro-BGA Assembly			Reliability Test Data for Characteristic Life $N_{63.2\%}$ (cycles):		
Ref	**PCB Type**	**Resin**	***95% Confidence Low Limit***	$N_{63.2\%}$	***95% Confidence Upper Limit***
01	Rigid	NR	192	201	211
02	Rigid	EB	1,803	2,193	2,666
03	Rigid	NR	1,146	1,217	1,292
05	Rigid	EB	1,680	2,008	2,401
06	Rigid	EB	3,605	4,020	4,483
08	Rigid	UN	13,312 cycles with no failure		
10	Compliant A	NR	917	953	990
11	Compliant B	NR	2,372	2,464	2,559
14	Compliant A	EB	10,992	14,013	17,864
15	Compliant B	EB	8,948	13,560	20,548
18	Compliant A	UN	11,980 cycles with no failure		
19	Compliant B	UN	6,880 cycles with no failure		

As detailed in Table II, over the reported number of TCs none of the underfilled assemblies has failed during the duration of the test (Ref 08, 18 and 19, number of components under tests for each variant was 28).

D. Experimental Results: Findings and Discussions

The outcomes from the experimental tests provided evidence that the assembly cases without any adhesive resin have overall the lowest lifetime. Among these, only the design with the compliant material B (Ref 11) offsets to some extent the impact from the CTE mismatch between the rigid board and the package on solder joint reliability. An unexpected result is that the PCB with the low-modulus compliant layer A (Ref 10) did not improve the reliability compared with the all-rigid board assembly (Ref 3). This outcome was further investigated using the results from the respective thermo-mechanical simulation.

At the other end, the use of underfill provided a very large improvement across all board variants. For the duration of the TC tests, no failure across these assemblies (Ref 08, 18, 19) has occurred. Even with the expected to be least reliable rigid design variant, Ref 08.

Assemblies with edgebond have also improved the reliability compared with the no resin variants although not as much as the underfill. The reliability is strongly enhanced when the edgebond is applied with any of the two complaint PCBs (Ref 14 and 15).

Although limited to one board (rigid) and a single resin (EB) design configuration, the test programme also provided a useful insight into the improvement offered by the dual ball redundancy design (Ref 06) compared with the µBGA assembly variant with no redundant balls (Ref 05). In this instance an improvement in lifetime by a factor 2X was identified. In the context of PCB land type effects, the µBGA assembly becomes extremely unreliable (worst lifetime among all cases) when the attachment of the package is on a board with SMD pads and without any resin (Ref 01). The type of PCB land type (SMD vs NSMD) seems to have smaller impact on the solder joint reliability if resin is used (the assembly variants with edgebond, Ref 02 and 05, but arguably similar outcome for the cases of underfilled assemblies).

III. THERMO-MECHANICAL SIMULATIONS

A. Finite Element Modelling for Stress Analysis and Solder Joint Damage Predictions

The finite element modelling work for the µBGA assembly has been previously reported by the team and therefore will be only summarised in this section [13]. Although the package does not feature exact quarter symmetry in terms of the layout of the balls in the array, a modelling investigation has confirmed that the difference in the predicted solder joint damage (thermally induced fatigue) obtained from a full-scale model and from a quarter symmetry model is very small across all joints (<1.7%). This has justified the deployment of a quarter assembly model which has reduced the computational time of the undertaken simulations and the analysis of the µBGA assembles listed in Table I. Illustrations of the three-dimensional finite element models representing a quarter section of the resin-based µBGA assemblies are shown in Fig. 5 and Fig. 6, for the edgebond and underfill variants, respectively.

The model alternations to capture the PCB board type, specifically the two compliant board designs featuring complaint layers utilising the two different materials, A and B, are detailed in Fig. 7.

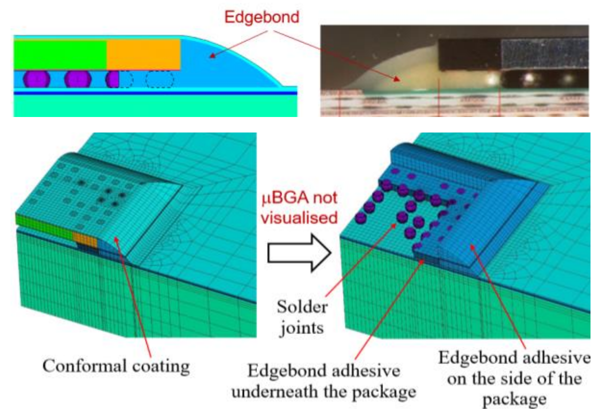

Fig. 5. Finite element model of µBGA assembly with edgebond. The model assumption is for edgebond penetration line half-way through the second row of solder joints.

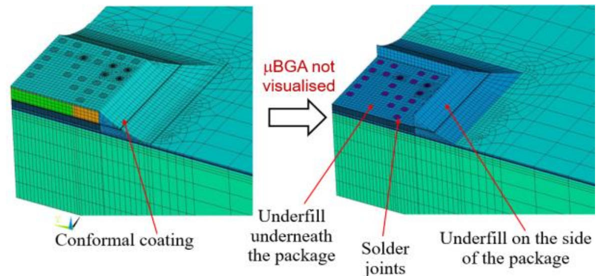

Fig. 6. Finite element model of µBGA assembly with underfill.

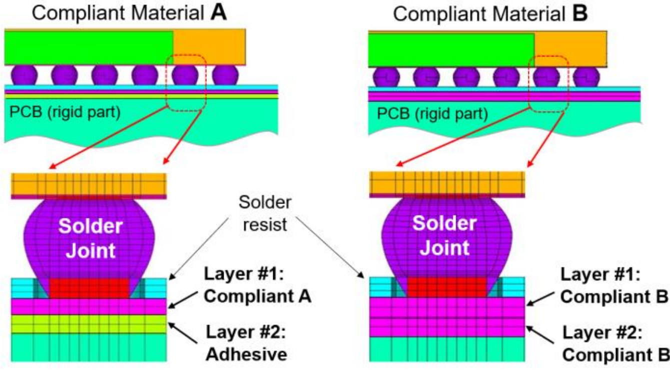

Fig. 7. Specification and modelling representation of compliant layers in the PCB board. The layer of compliant material A requires an adhesive layer to add to the PCB laminate stack while the compliant material B has an equivalent (thickness-wise) application of two layers of the same material.

Non-linear transient thermo-mechanical analysis is performed to simulate the stress response of the µBGA assembly under temperature cycling for each assembly case. Temperature dependant elastic material behaviour is assumed for all materials except for the quaternary alloy SnPbAgCu composition [14]. The solder is modelled as a visco-plastic material using the Anand constitutive law [13]. The temperature cycle profile used in the experimental tests was applied as an isothermal load. Three temperature cycles were simulated to provide a stabilised hysteresis loop and a prediction for the inelastic strain energy density (plastic work) in the solder joints accumulated over one temperature cycle.

B. Model-based Calculation of Solder Joint Damage

The finite element simulations provided predictions for the plastic work in the solder joints accumulated over one temperature cycle (ΔW_p). As detailed in Fig. 8, each solder joint is modelled with an explicit volumetric layer, with thickness 20 µm, at both the PCB and the package side pad interfaces (notation V^b and V^t, respectively). These are the expected locations for solder crack initiation and propagation, as confirmed with the cross-sectional analysis of experimentally failed joints. These interfacial layers are used to calculate volume-weighted average values (interfacial damage values) of the plastic work, $\Delta W_{ave}^{i},\ i = \{t, b\}$, at the top (t) and bottom (b) interfaces of the solder joints using 20% sub-volumes in V^t and V^b. These 20% sub-volumes are defined by the mesh elements with the highest plastic work within V^t and V^b, respectively, which reduces the level of plastic work distribution non-uniformity [13]. This approach has been informed by previous work by Che and Pang showing that the common approach of averaging over an entire solder joint interfacial layer volume can underestimate the strain energy density when correlating to solder joint fatigue life data [4].

The damage value for a given solder joint, ΔW_{ave}^{joint}, is defined as the largest from the two damage values associated with the top and bottom solder joint interfaces:

$$\Delta W_{ave}^{joint} = max\{\Delta W_{ave}^{t}, \Delta W_{ave}^{b}\} \quad (1)$$

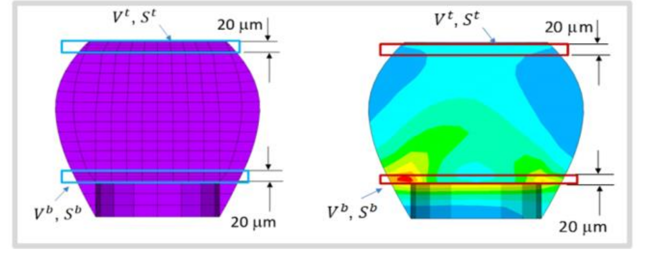

Fig. 8. Solder joint mesh density and volumetric interfacial joint layers used in the calculation of the solder damage value.

For the µBGA assemblies without redundant ball design (Ref. 01, 02 and 05), the most critical joints in the array that can fail first and lead to overall assembly failure are joints #1, #3 and #5. The locations of these joints are detailed in Fig 9. For the dual ball redundant design, the most critical connections are the non-redundant joint #1 and the dual-ball redundant pairs of joints (#2,#3) and (#4,#5) (refer to Fig. 9). In this instance, a package failure caused by a redundant pair of connections requires both solder joints to fail. The solder joints at the package corner and in the peripheral rows (the dark solid blue balls in the schematic) are non-critical and their cracking will not result in failure of the µBGA. Therefore, the damage value used to predict the failure of a µBGA assembly (ΔW) for the non-redundant design (single ball/net) is

$$\Delta W = max\{\Delta W_{ave}^{\#1},\ \Delta W_{ave}^{\#3},\ \Delta W_{ave}^{\#5}\} \quad (2)$$

and for the dual ball/net assembly design is defined as

$$\Delta W = max\left\{\Delta W_{ave}^{\#1}, min\{\Delta W_{ave}^{\#2}, \Delta W_{ave}^{\#3}\}, min\{\Delta W_{ave}^{\#4}, \Delta W_{ave}^{\#5}\}\right\} \quad (3)$$

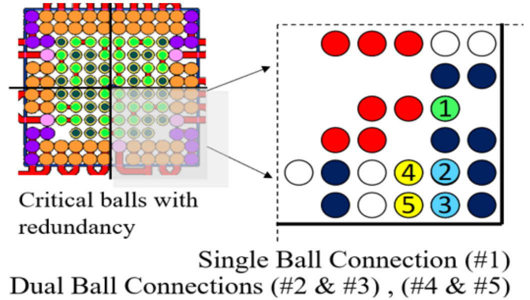

Fig. 9. Layout of solder balls and the dual ball interconnections (redundancy) in orange (left), and the model assessed joints #1 to #5 in the quarter section of the assembly (right) .

C. Demonstration of Solder Damage Modelling Results

For each assembly case in Table II, modelling predictions for ΔW_{ave}^{joint} are obtained for all five joints of interest (Fig. 9, right). These results are then used with Eq. 2 and 3 to identify the joint to which the failure of the µBGA is attributed and the respective ΔW. As a demonstration of the damage assessment procedure, the modelling results for the solder joint reliability only for the rigid board and no resin assembly case Ref 03 are outlined. Fig. 10 (top) shows the contour plot of the most critical solder joints that are investigated (#1-#5), informing that the location of

highest damage within a joint and hence the expected crack location is at interface with the package. The solder joints damage order, based on the calculated values for ΔW_{ave}^{joint}, is given with the graph at the bottom of Fig. 10. The results identify the dual ball connection (#2,#3) as the one failing first, and hence the µBGA failure is associated with the failure of joint #2 (it follows the failure of joint #3 in the dual connection). Therefore, for Ref 03 the assembly failure is associated with the solder damage of joint #2, and ΔW=0.3818MPa. More results are detailed in reference [13].

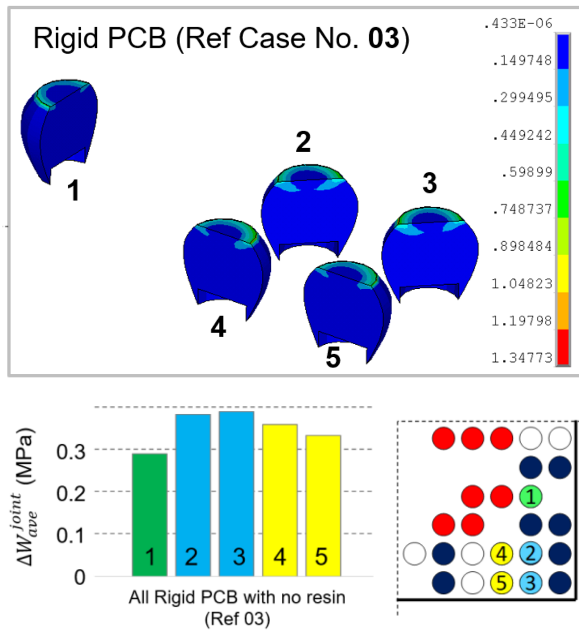

Fig. 10. Contour plot of the plastic work ΔW_p (J/cm^3, or MPa) for the five critical joints of interest with the Ref 03 assembly (top) and their respective solder damage values (bottom).

Fig. 11 provides a normalised plot of the solder damage values ΔW indicative for the failure of the dual ball, NSMD assembly variants (normalised value 1 given by ΔW=0.3935 MPa) . The no-resin assembly gives the lowest reliability. The solder damage is driven by shear deformation caused by the global, in-plane CTE mismatch between the PCB and the package. The relative ranking of solder damage is explained with differences in the elastic modulus (rigid dielectric material stiffer than the compliant materials) and how close the µBGA composite CTE (6-7 ppm/°C) is matched by the CTEs of the PCB and its topmost layer – this being a rigid dielectric (CTE<15 ppm/°C) or a compliant material (CTE>20 ppm/°C for material A and CTE<10 ppm/°C for Material B) [13].

In the case of µBGA assemblies with edgebond, it is observed that the location of higher damage is at the interface with the PCB pad for the solder joints that are fully encapsulated by the edgebond (i.e. peripheral rows). For the joints in the second row, assumed to be partly encapsulated, plastic work concentrations are predicted at both the PCB interface (solder and edgebond boundary region) and at the package side (solder joint side not interfacing with the edgebond). The interfacial location for highest solder damage was found to depend on the degree of penetration of the edgebond in relation to the joint.

The underfill application is predicted to reduce substantially the solder damage. The predicted crack location is at the PCB side of the joints. The compliant PCB designs with underfill are predicted to provide greater life improvement compared with the rigid PCB. For both edgebonded and underfilled assemblies, this is explained with the positive role of the resin in reducing the global level CTE mismatch (in-plane shear).

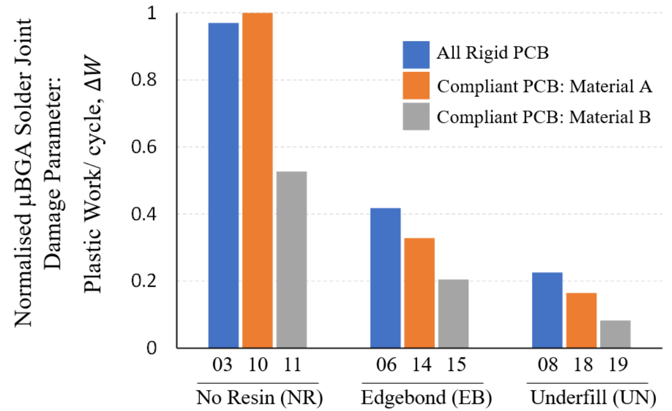

Fig. 11. Assembly optimisation: modelling predictions for solder joint damage (normalised values) with NSMD, dual ball redundant assembly variants deploying rigid and compliant PCB variants, and different no resin and resin (underfill, edgebond) solutions.

Although limited, an insight into the sensitivity of solder damage to the degree of edgebond penetration beneath the package is obtained through a parametric study using the assembly Ref 02. The parametric study is limited to modelling of the local penetration effect in relation to the solder joint #1 (Fig. 12) which was predicted to be the failure joint for that assembly case. Three scenarios are assessed (Fig. 12):

- Ref 02(a) : The nominal case assuming edgebond penetration halfway through the solder joints in the second row, resulting in 50% joint #1 encapsulation.
- Ref 02(b) : 75% encapsulation of joint #1 locally.
- Ref 02(c) : Full (100%) encapsulation of joint #1 locally.

The modelling predictions show a very strong sensitivity of the predicted solder damage to the level of edgebond joint encapsulation, even under the assumption the penetration is local and affecting only joint #1. The solder damage is lowest when the solder joint is fully surrounded by the edgebond material (case 02(c)), and the damage is highest for the case 02(a):

- Ref 02(a): $\Delta W_{ave}^{\#1} = 0.5489$ MPa
- Ref 02(b): $\Delta W_{ave}^{\#1} = 0.3363$ MPa
- Ref 02(c): $\Delta W_{ave}^{\#1} = 0.2043$ MPa

While the edgebond penetration effect is simulated only for the assembly Ref 02, the results indicate that the modelling predictions for the µBGA assemblies that use the resin solution with the edgebond are strongly influenced by the assumption made on the degree of edgebond penetration. This is a factor that can influence the correlation between the model predicted solder

damage values and the experimentally gathered failure data for the edgebond assemblies.

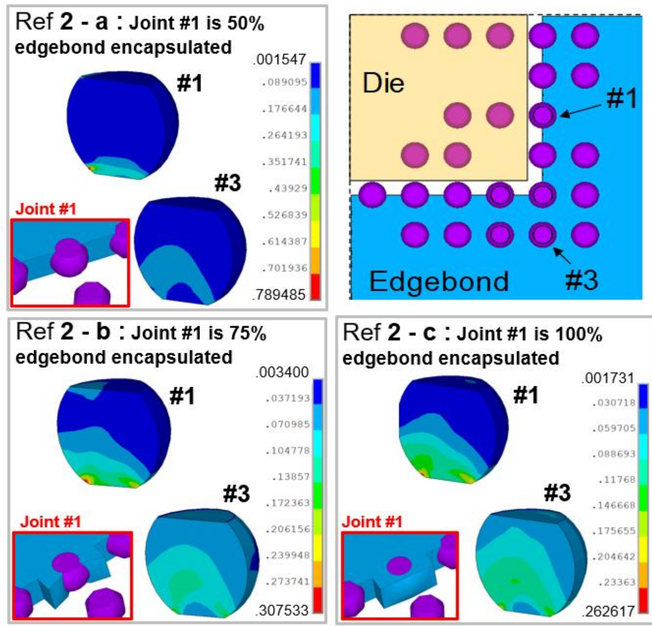

Fig. 12. Parametric cases for local level edgebond penetration and solder joint encapsulation (solder joint #1) on induced thermal fatigue damage. Contour plots show the modelling predictions for plastic work (MPa) in solder joints #1 and #3 accumulated over one temperature cycle.

IV. Fatigue Life Prediction Model for micro-BGAs

The availability of experimentally derived thermal fatigue failure data and the related modelling predictions for solder joint damage provide the opportunity to correlate this data and to derive a thermal fatigue lifetime model for predicting the cycles to failure of solder joints with mixed SnPbAgCu alloy composition. The plot of the log-log data correlation (ΔW vs. $N_{63.2\%}$) is shown in Fig.13.

The correlation between the model and the no resin assembly data (Ref. 01, 03, 10 and 11) is found to be very good. The location of the data points of the edgebond assemblies (Ref. 02, 05, 06, 14, 15) in the plot are potentially less certain. A contributing factor for that is the possible variation in the edgebond penetration with the real assemblies and the deterministic assumption for this parameter made in the model. As an example, for assembly Ref 02 we provide the horizontal error bar (red line) which shows the variation range for the predicted solder joint damage when the edgebond penetration level (even locally, as detailed in the previous section) changes in the vicinity of the critical solder joint. Although we have not quantified explicitly the edgebond penetration effects on the predicted plastic work in the solder joints with the other edgebond assemblies, the result for Ref 02 and past research on the impact of conformal coating penetration beneath the package edges [8] suggest that such sensitivity will be present.

In the graph of Fig. 13 two more assemblies (Ref 14 and 15) are included with error bars. These vertical error bars show the 95% confidence interval for the prediction of the characteristic life obtained from the Weibull data distribution. This life range is indicated in the plot because the failure datasets for these two assembly variants feature large number of censored data; the confidence intervals for the estimated characteristic life are therefore significantly wider compared with the other assembly variants. Although the modelling predictions identified that the edgebond assembly with the complaint PCB material B (Ref 15) is more reliable than the one with the compliant material A (Ref 14, see Fig. 11), the reliability tests, despite the wider CIs for the characteristic life, identified that the two assemblies may have similar lifetime. There is no simple explanation of why that may be the case. In addition to the edgebond penetration factor, it may be the case that the long application of the cycling load (See Fig. 4 cycle count) had an aging impact on the materials which has not been captured with the model assumed edgebond material behaviour and properties.

There are no underfill assembly data points in the graph because no failures occurred with these assemblies. Among the three PCB variants for the underfill assembly, based on the modelling predictions (Fig. 11) and related knowledge about the rigid vs. complaint PCBs performance, it would be expected that the rigid PCB variant will be the least reliable. Yet, the underfilled assembly with the rigid PCB has reached >13,000 cycles without any failure recorded. Both the modelling predictions and the reliability tests agree that an exceptional reliability performance and maximum reliability will be achieved with the application of an underfill. However, the lifetime model defined with the regression line in Fig. 13 is currently underestimating the lifetime of the Ref 08 assembly (model prediction for $N_{63.2\%}$ =12,037 cycles while test outcome is for no failures even after 13,000 cycles). A possible reason is that the long life of these assemblies might have time dependant effect on the underfill behaviour, and the reasonable modelling assumption for elastic material behaviour to be less certain as a result in this instance.

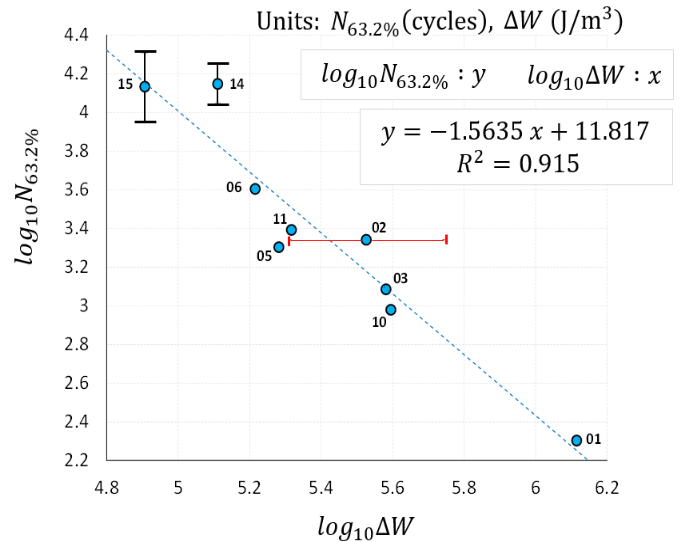

Fig. 13. Log-log plot of model predictions for solder thermal fatigue damage ΔW (model) vs. characteristic life (test failure cycles). Data correlations used to derive a thermal fatigue lifetime model for quaternary alloy SnPbAgCu solder composition in the form of a power law relation, $N_{63.2\%} = A(\Delta W)^B$.

V. CONCLUSIONS

This paper detailed the results from an experimental program and the related thermo-mechanical modelling for (1) assessing SnPbAgCu solder joint fatigue reliability performance for the μBGA architecture and (2) optimising the package-board assembly design for safe deployment in high-reliability applications. New knowledge and insights into the impact of several assembly designs and assembly materials on the lifetime of this chip-scale package type were reported and can act as guidelines for assuring a safe deployment of the package in electronic systems operated under harsh environment conditions. The findings from this study informed that without the development of enhanced, stress-reducing assembly designs, the reliability of the μBGA may not meet the stringent lifetime requirements posed by many high-reliability applications.

The outcomes from the reported comprehensive reliability testing of the μBGA package under accelerated temperature cycling load, using twelve different assembly designs, confirmed a major variation in the observed thermal fatigue performance of the solder joints. Depending on the assembly design, characteristic life of solder joints can be extended from as little as 200 cycles to a minimum failure-free life in order of 13,000 cycles. Least reliable is the no-resin design with an all rigid (dielectric material) board designed with solder mask defined lands and without ball redundancy. Based on gathered TC tests data, the no resin μBGA assemblies may not satisfy typical high reliability specifications.

Both edgebond and underfill material application provide a notable improvement of the solder joint fatigue life but the use of underfill is more beneficial. The edgebond application requires special attention and robust control to avoid uncertainty and variation in the penetration beneath the package, which in turn can affect the solder joint reliability. PCBs designed with compliant layers can offer further benefits and reduce the CTE mismatch-induced stresses in the solder joint, and hence can also extend the lifetime. The compliant material selection is not trivial and requires careful selection. The results demonstrated that an optimised combination based on underfill and/or compliant PCB, with all other assembly attributes unchanged, can provide solder joint life improvement by factor >10X compared with the "conventional" no resin assembly on an all-rigid PCB. While the use of underfill is superior compared with the edgebond and no resin solutions, an important consideration is whether the underfill is reworkable or not. The deployment of a reworkable edgebond material may be preferable to a non-reworkable underfill, particularly when used in combination with a compliant PCB, if the required reliability performance can be met.

Solder damage predictions from physics-of-failure modelling are found to be in a good agreement with the experimental failure data. Such models can be deployed upfront as design tools to assess the reliability performance of different designs and to generate results to guide the design optimisation at package assembly level. A major output form this work is the development of a fatigue lifetime model for SnPbAgCu solder joints of μBGAs and similar CSP components.

ACKNOWLEDGMENT

The authors thank Leonardo UK Ltd. (Edinburgh) for providing access to the μBGA assembly designs and the reliability test data, and their Graeme S. Tough for preparing microsections and conducting EDAX examinations. We also thank Graeme Morrison and Dr Chunyan Yin for their contributions to the technical and modelling aspects of the study, respectively.

REFERENCES

[1] M.-C. Hsieh, "Simulations and characterizations for stress reduction designs in Wafer Level Chip Scale Packages," Proc. Inter. Microsystems, Packaging, Assembly and Circuits Technology Conference (IMPACT), Taipei, Taiwan, pp. 230-233, Oct. 2013.

[2] X.J. Fan, B. Varia, and Q. Han, "Design and optimization of thermo-mechanical reliability in wafer level packaging," Microelectronics Reliability, vol. 50 (4), pp. 536-546, April 2010

[3] P. Limaye, B. Vandevelde, J. Van de Peer, S. Donders and R. Darveaux, "Probabilistic design approach for package design and solder joint reliability optimization for a lead free BGA package," Proc. International Conference on Thermal, Mechanical and Multi-Physics Simulation and Experiments in Micro-Electronics and Micro-Systems, Berlin, Germany, 18-20 April 2005, pp. 531-537.

[4] F.X. Che and J.H.L Pang, "Fatigue reliability analysis of SnAgCu solder joints subject to thermal cycling", Proc. IEEE Trans. on Device and Materials Reliability, Vol. 13, No. 1, pp. 36-49, March 2013.

[5] S. Stoyanov, C. Bailey, and M. Desmulliez, "Optimisation modelling for thermal fatigue reliability of lead-free interconnects in fine-pitch flip-chip packaging," Soldering and Surface Mount Technology, vol. 21 (1), pp. 11-24, Feb 2009

[6] E.H. Wong, W.D. van Driel, A. Dasgupta, and M. Pecht, "Creep fatigue models of solder joints: A critical review," Microelectronics Reliability, vol. 59, pp 1-12, April 2016

[7] M. Serebreni, R. Wilcoxon, F. Patrick McCluskey, "Modelling the influence of conformal coatings on thermo-mechanical fatigue of solder interconnects in electronic packages," Proc. IMAPS High Temperature Electronics Conference (HiTEC), 000007, pp 1-8, May 2018.

[8] C. Yin, S. Stoyanov, C. Bailey, P. Stewart, "Thermomechanical analysis of conformally coated QFNs for high-reliability applications," IEEE Trans. on CPMT, Vol. 9, No. 11, pp. 2210-2218, Nov. 2019.

[9] T. Bo, Y. Zhouping, D. Han, and W. Yiping, "Reflow profile optimization of μBGA solder joints considering reflow temperature and time coupling", Soldering & Surface Mount Technology, vol. 21 (4), pp. 38-44, Sep 2009

[10] H. Chen, T.-T. Chou, C. Fleshman and J.-G. Duh, "Investigating the effect of Ag content on mechanical properties of Sn-Ag-Cu micro-BGA joints," Journal of Electronic Materials, vol. 48, pp. 6866–6871, July 2019

[11] J. H. L. Pang, P. T. H. Low and B. S. Xiong, "Lead-free 95.5Sn-3.8Ag-0.7Cu solder joint reliability analysis for micro-BGA assembly," Proc. Intersociety Conference on Thermal and Thermomechanical Phenomena in Electronic Systems, Las Vegas, USA, 1-4 June 2004, pp. 131-136.

[12] U. Genschel and W. Meeker, "A comparison of Maximum Likelihood and Median-Rank Regression for Weibull estimation," Quality Engineering, vol. 22(4), pp. 236-255, August 2010.

[13] S. Stoyanov, C. Bailey, P. Stewart, and G. Morrison, "Reliability impact of assembly materials for Micro-BGA components in high reliability applications," Proc. IEEE Electronics System-Integration Technology Conference (ESTC), 15-18 Sept. 2020, 9229828, Sep. 2020

[14] Y. Zhang et al., "Analysis of the mechanical behaviour, microstructure and reliability of mixed formulation solder joints," Proc. ECTC, San Diego, CA, USA, pp. 759-770, May 2009.